DOI: 10.1109/tste.2019.2911453

Reactive Power Synchronization Method for Voltage Sourced Converters

Andrés Peña Asensio, Santiago Arnaltes Gómez, Jose Luis Rodriguez-Amenedo, *Member, IEEE* and Miguel Ángel Cardiel-Álvarez

***Abstract*—There is a growing interest in the parallel operation of Voltage Source Converters (VSCs) both in an isolated microgrid or connected to the utility grid. The most common solution in the literature for the paralellization of VSCs is the so-called droop control, which brings about a relationship between active power and frequency. In this paper, a different approach is proposed where reactive power is used instead of active power to ensure synchronous operation. Active and reactive power are independently controlled using a dq-frame representation based on the vector oriented control, which inherently provides current limitation capability. A detailed dynamic model of the system is used to demonstrate the relation between reactive power and frequency. Due to the intrinsic synchronizing mechanism, the proposed scheme can operate in both isolated and grid-connected modes. As opposed to droop control schemes, active power is not used for synchronization and thus synchronization is possible even if active power is not controllable. Simulation and experimental results, for a case study where a VSC is connected to a host grid, are presented to validate the proposal.**

***Index Terms*—Power generation control, droop control, synchronous power controller, distributed control.**

I. Introduction

VOLTAGE Sourced Converters (VSCs) are the most common way of interfacing distributed generation and energy storage systems. They are becoming increasingly important for electrical systems due to the development of renewable energies and, recently, to the rising of microgrids.

Microgrids are usually defined as a set of loads, distributed generation and energy storage systems that operate as a single controllable system [1]. It is a very promising concept that could provide better reliability and efficiency to electrical distribution systems, especially remote ones. Moreover, they provide a promising frame for the integration of distributed renewable energy systems. However, their operation is strongly dependent on the converter control of their units, which must be adapted to their distributed nature [2].

One of the main features of VSCs is the possibility to independently control their active and reactive power. To perform this control, the generated voltage must be synchronized with the system they are connected to [3]. In a microgrid, this outer system could be an isolated load, a main grid or even other VSCs.

A. Peña, S. Arnaltes, J.L. Rodriguez and M.A. Cardiel are with the Department of Electrical Engineering, University Carlos III de Madrid, Leganes 28911 Spain (e-mail: anpenaa@ing.uc3m.es, arnalte@ing.uc3m.es, amenedo@ing.uc3m.es, mcardiel@ing.uc3m.es)

This work has been supported by the Autonomous Community of Madrid under the PRICAM project (S2013-ICE-2933).

A common approach, usually applied to grid-connected systems, is measuring the frequency by means of a Phase Locked Loop (PLL) [4], [5]. This ensures that the generated internal voltage has the same frequency as the grid voltage and the angle required for the power injection. However, PLLs are known to present problems when applied to islanded systems [6]. Moreover, traditional power systems have also been reported to present instabilities for high-penetrations non-synchronous generators, related to the use of PLLs [7]. The GB system operator, National Grid, is encouraging to seek alternatives to PLLs for converter-interfaced systems [8].

Another approach, commonly known as droop control, is to introduce a relationship between the VSC active power and frequency [9]–[13].

It has been demonstrated how it is possible to synchronize multiple VSCs when they operate using this strategy [14]. This is due to the emulation of synchronous generators synchronizing torque, which introduces a negative feedback of the phase displacement, ensuring that mechanical forces will be set up to restore the rotor angle of the machine following an arbitrarily small displacement of this angle [15].

A more precise emulation of the synchronous machine operation has also been proposed through the Virtual Synchronous Machine (VSM) concept [16], [17]. A similar approach, called power synchronization control (PSC), is introduced in [18] for the case of grid-connected HVDC systems.

All of these implementations have in common the use of a dependency between active power and frequency as synchronizing mechanism [19], [20]. Therefore, the synchronism is not possible if the active power required by the synchronizing mechanism is not controllable, since the power/frequency droop will require active power sharing that cannot be guaranteed.

In this paper, a different approach is proposed where reactive power is used instead of active power for the synchronous operation of VSCs, thus decoupling the synchronization mechanism from the VSC active power, while no PLL is required for frequency measurement.

This proposal is based on a dynamic modeling of a grid-connected VSC from a new perspective that shows a dynamic coupling between the VSC reactive power and power angle, and therefore between reactive power and frequency. The relation between reactive power and frequency has been addressed in previous publications but with different purposes.

In [21] the authors propose a frequency-reactive power control in order to share the reactive power among different converters in a microgrid. This frequency-reactive power con-

trol is not used for synchronization. Instead, an unspecified frequency measurement unit is used to orientate the internal variables.

In [22] the authors propose a modified droop control for load-sharing between UPS systems that uses a virtual resistive output impedance. Given a total resistive output impedance, the static relation between reactive power and frequency on resistive networks is used to propose a frequency-reactive power droop control that improves damping and reactive current sharing compared to previous solutions. A similar approach is presented in [23]

In this paper, reactive power is used for grid synchronization so a frequency measurement unit, such as a PLL, is not required. The impedance is not assumed or virtually modified to be resistive and the sensitivity for different inductive to resistive ratios is addressed. Active and reactive power are independently controlled using a dq-frame representation based on the vector oriented control (VOC) scheme. VOC inherently provides several known features such as current limitation capability.

In section II the proposed control system is presented and explained using a simplified model. A more detailed state-space model is presented in section III. This analysis method has also been applied to droop [24], [25] and VSM [19] control systems. The eigenvalue analysis is performed in section III-B to evaluate the system performance.

Experimental and simulation results, for a case study where a VSC is connected to a host grid, are presented in section IV to validate the proposal.

II. Proposed Control

In this section, the proposed control system is presented. A small-signal model of a grid-connected VSC is used to demonstrate the relation between reactive power and phase displacement. An analogy with the swing equation of traditional power systems, based on synchronous generators, is presented to illustrate the synchronizing system.

A general scheme of the proposed control system is depicted in Fig. 1. The control system is based on a dq-frame representation of the system voltages and currents. The reference for this dq-frame is obtained from a novel synchronization mechanism based on the measurement of the exchanged reactive power. The inputs of this control system are the active current $i_d{}^*$ and the reactive power q^* references, both of which can be independently controlled.

Variables in lowercase are represented in pu with respect to the base values included in Table I. These values were selected considering the set-up used for the real time experiments that will be presented in section IV.

TABLE I
Base values for per unit transformations

Label	Value	Units	Description
U_b	400	V	AC base voltage (rms)
$U_{dc,b}$	$2U_b$	V	DC base voltage
S_b	20	kVA	Base power
f_b	50	Hz	Base frequency
Ω_b	$2\pi f_b$	rad/s	Base angular frequency

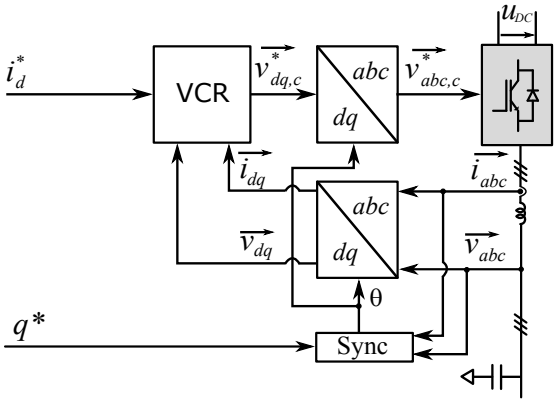

Fig. 1. General scheme of the proposed control and system under study. VCR: Voltage and Current Regulation.

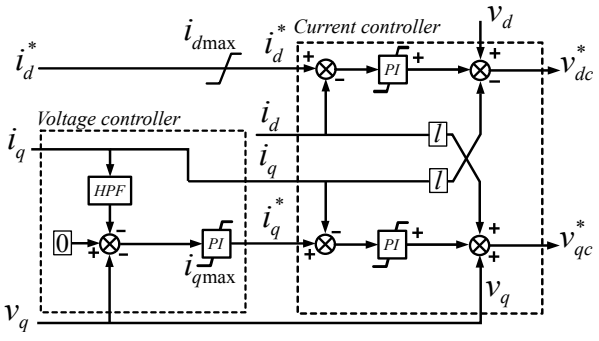

Fig. 2. Internal Voltage and Current Regulation (VCR) system. HPF: High-pass filter.

The internal Voltage and Current Regulation (VCR) system of Fig. 1 is based on the classical current vector control. A more detailed scheme is depicted in Fig. 2. As in current vector control, it is possible to decouple active and reactive current control as well as limit the current injected by the VSC.

A high-pass filter (HPF) is included in the voltage controller of Fig. 2 as an oscillation damping mechanism. This will be further discussed in section III-C.

A. Reactive power synchronization concept introduction

Traditionally, as an approximation to synchronous generators, a relation has been established between a VSC active power generation and its frequency [16], mimicking the behavior of synchronous generators synchronizing torque. However, in VSCs there is no relation between the phase of electrical variables and a mechanical system requiring a force to restore position. Accordingly, there is no intrinsic need of relating active power to phase displacement in order to synchronize the system.

Another argument for using active power for the synchronous operation of VSCs is the relationship between transmitted active power and power angle in power systems. Most studies use this relationship for synchronizing based on a steady-sate model of the grid short circuit impedance. On the other hand, in this paper a detailed dynamic model of a VSC connected to a host grid is used to demonstrate the relationship

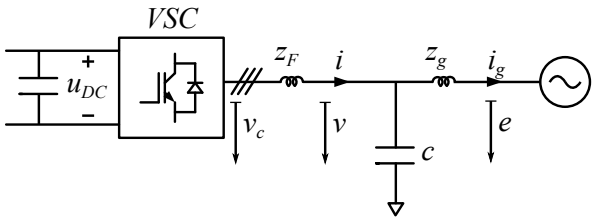

Fig. 3. Case study scheme. VSC: Voltage Sourced Converter.

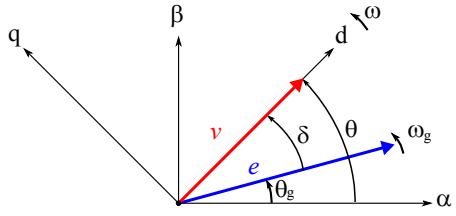

Fig. 4. Vector diagram of the system under study. δ: power angle. e: grid voltage vector. v: converter voltage vector. w: dq frame angular frequency. w_g: grid frequency.

between phase displacement and reactive power that it is the basis of the proposed synchronizing method.

The system under study is depicted in Fig. 3. It represents a VSC connected to grid through an LC filter and an interfacing impedance z_g.

The power angle δ can be defined from the dq-frame angular frequency w and the grid frequency w_g as

$$\frac{1}{\Omega_b}\frac{d\delta}{dt} = \omega - \omega_g \tag{1}$$

A graphical representation of these variables together with the grid voltage vector e and converter voltage vector v is depicted in Fig. 4.

The internal VCR system of Fig. 2 is responsible of tracking the active current reference ${i_d}^*$ and also of keeping the internal voltage vector aligned with the reference frequency ω, which is achieved by a regulation of the quadrature component of the capacitor voltage v_q [26]. The dynamics of this internal VCR loops are usually faster than the synchronizing system loop so it can be assumed that

$$i_d = {i_d}^* \tag{2}$$
$$v_q = 0 \tag{3}$$

This assumption will be validated in section III. The relationship between the VSC and grid voltages is given by

$$\frac{l_g}{\Omega_b}\frac{d\vec{i_g}}{dt} = \vec{v} - \vec{e} - r_g\vec{i_g} - j\omega l_g\vec{i_g}, \tag{4}$$

where i_g is the current flowing through the grid impedance $z_g = r_g + j\omega l_g$ as seen in Fig. 1. Given (2) and (3), active and reactive power delivered by the VSC to the grid can be defined as

$$p = i_{dg}v_d \tag{5}$$
$$q = -i_{qg}v_d \tag{6}$$

From (6), it can be seen that reactive power q is related to i_{qg}. From (4), it is obtained that

$$\frac{l_g}{\Omega_b}\frac{di_{qg}}{dt} = -e_q - r_g i_{qg} - \omega l_g i_{dg} \tag{7}$$

From Fig. 4, it can be seen that e_q is related to the phase displacement δ as

$$e_q = -|e|\sin\delta \tag{8}$$

This introduces a non-linear relationship in (7). A small-signal model will be considered. A base case operating point for linearization is defined in Table II.

TABLE II
BASE CASE OPERATING POINT IN PU

Label	Value	Description
e_0	1	Grid voltage vector amplitude
w_{g0}	1	Grid voltage frequency
i_{d0}	1	VSC active current generation
q_0	0	VSC reactive power generation

Linearizing (7) around this operating point leads to

$$\frac{l_g}{\Omega_b}\frac{d\Delta i_{qg}}{dt} = e_0\cos\delta_0\Delta\delta - r_g\Delta i_{qg} - \omega_0 l_g\Delta i_{dg}, \tag{9}$$

where the product $i_{qg0}\Delta\omega$, which depends on the synchronizing mechanism, has been neglected. Equation (9) shows that there is a dependency between i_{qg}, or reactive power, and the power angle δ.

Note that if only the steady-state is considered, neglecting $\frac{d\Delta i_{qg}}{dt}$ in (9), it will follow that only Δi_{dg}, or active power, is related to δ, as is commonly stated. Therefore, from (9) it is concluded that, although there is no steady-state relation between reactive power and phase displacement, there do exist a dynamic relation.

To clarify the explanation, the filter capacitor is not considered here. Therefore, based on (2) it is deduced that $\Delta i_{dg} = \Delta {i_d}^*$. From (9) it can be written that

$$\Delta i_{qg} = \frac{\omega_0 l_g}{\frac{l_g}{\Omega_b}s + r_g}\left(\frac{e_0\cos\delta_0}{\omega_0 l_g}\Delta\delta - \Delta {i_d}^*\right) \tag{10}$$

For reactive power, based on (6) and for the operating point defined in Table II, it is obtained that

$$\Delta q = \underbrace{\frac{\omega_0 l_g}{\frac{l_g}{\Omega_b}s + r_g}}_{G_{qp}}\left(\Delta p^* - \underbrace{\frac{v_{d0}e_0\cos\delta_0}{\omega_0 l_g}}_{G_{p\delta}}\Delta\delta\right), \tag{11}$$

where $\Delta p^* = v_{d0}\Delta {i_d}^*$. Note that $G_{p\delta}$ is in fact the commonly considered coupling between active power and power angle, while G_{qp} represents the coupling between active and reactive power through the dynamics of the grid inductance.

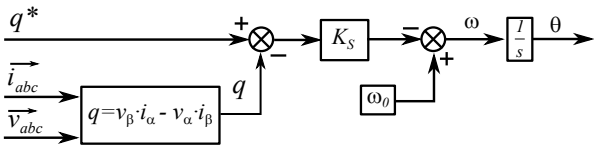

Fig. 5. Reactive power synchronization loop.

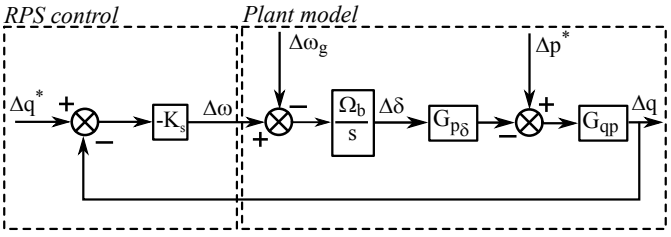

Fig. 6. Block diagram of the complete system. RPS: Reactive Power Synchronization.

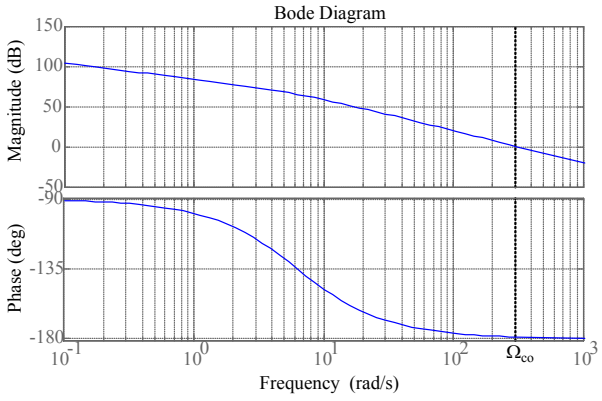

Fig. 7. Bode diagram of the open-loop transfer function for the reactive power synchronization model. Ω_{co}: Cross-over frequency.

B. Description of the reactive power synchronization control

Equation (11) demonstrates that phase displacement variations are related to reactive power and consequently that reactive power can be used as a synchronizing mechanism.

Considering this coupling, the proposed control system is depicted in Fig. 5. The internal frequency of the control system ω is defined by the control law

$$\omega = \omega_0 - (q^* - q) * K_s, \tag{12}$$

where ω_0 and K_s are the control parameters and q^* is the VSC reactive power set-point.

With this system, the VSC will deliver a reactive power q^* if the frequency is w_0, but otherwise reactive power will vary proportionally to the frequency deviation. Thus, synchronization can be independent of active power generation.

The small-signal block diagram, including the proposed control system and the plant model, is depicted in Fig. 6. The resulting open loop transfer function can be obtained combining equations (1), (11) and (12) as

$$G_{OL} = \frac{K_s \Omega_b v_{d0} e_0 \cos\delta_0}{s(\frac{l_g}{\Omega_b} s + r_g)} \tag{13}$$

A bode diagram of this transfer function is presented in Fig. 7, for the base case parameters given in Table III.

TABLE III
BASE CASE SYSTEM PARAMETERS IN PU

Label	Value	Description
l_f	0.2	Filter inductance
r_f	0.003	Filter resistance
c	0.05	AC capacitance
l_g	0.1	Grid inductance
r_g	0.001	Grid resistance
c_{DC}	0.35	DC capacitance
k_{pc}	2	AC current proportional gain
k_{ic}	0.637	AC current integral gain
k_{pv}	2.5	AC voltage proportional gain
k_{iv}	0.127	AC voltage integral gain
k_s	0.1	Synchronization loop gain

The open-loop transfer function already comprises a good reference-tracking behavior, due to the intrinsic integrator, and thus a proportional controller is enough to ensure synchronous operation. If the system is stable, $\Delta\omega = \Delta\omega_g$ and the VSC will be operating in synchronism with the grid. For the given parameters, the cross-over frequency is located at

$$\Omega_{co} = \Omega_b \sqrt{\frac{K_s}{l_g} v_{d0} e_0 \cos\delta_0} \quad , \tag{14}$$

discarding the effect of r_g.

Both active power and grid frequency variations act as perturbations of the proposed control system. Thus, the angle varies to reject active power variations, allowing the system to remain in synchronism regardless of the required power angle. In contrast, when using active power for synchronization, as in PSC, the active power reference must be varied in order to change the power angle, which is usually performed by an outer DC-voltage control loop [18].

Also, it is worth noting that there is no need to measure the grid frequency which improves the robustness of the method over classical PLLs.

C. Characteristic swing equation

In this section the model of the reactive power synchronization control system is analyzed from the point of view of the characteristic swing equation, in an analogy to the operation of synchronous generators.

From the block diagram of Fig. 6, considering only the effect of active power variations, i.e. considering $\Delta\omega_g = 0$ and $\Delta q^* = 0$, it can be written that

$$\Delta p^* = \frac{1}{G_{qp} K_s \frac{\Omega_b}{s}} \Delta\delta + G_{p\delta} \Delta\delta \tag{15}$$

and considering (11)

$$\frac{1}{K_s {\Omega_b}^2} s^2 \Delta\delta + \frac{r_g}{\omega_0 l_g K_s \Omega_b} s\Delta\delta + G_{p\delta}\Delta\delta = \Delta p^* \tag{16}$$

which is analogous to the synchronous machine swing equation

$$\frac{2H}{\Omega_b} s^2 \Delta\delta + \frac{D}{\Omega_b} s\Delta\delta + K\Delta\delta = \Delta p_m \tag{17}$$

where H is the inertia constant, D the damping constant, K the synchronizing component and p_m the input mechanical power. For the proposed system

$$H = \frac{1}{K_s \Omega_b} \tag{18}$$

$$D = \frac{r_g}{\omega_0 l_g K_s} \tag{19}$$

$$K = \frac{v_{d0} e_0 \cos \delta_0}{\omega_0 l_g} \tag{20}$$

Note that, as in synchronous generators, the synchronizing torque component K in equation (20) is proportional to the grid strength.

III. Modeling and Analysis

In this section the system presented in Fig. 3, including the control system of Fig. 1, is modeled in the state space discarding the assumptions made in section II.

In order to assess the dynamics and stability of the overall system, the eigenvalue and sensibility analysis of this model are also performed. Since the system is non-linear the operation point also affects the stability of the system. The base-case operating point values are given in Table II.

A. State-space model

Using a transformation to a dq-frame rotating at ω, as depicted in Fig. 4, the VSC terminal voltage v_c and the capacitor bank voltage v are related by the equation

$$\vec{v} = \vec{v_c} - R\vec{i} - L\frac{d\vec{i}}{dt} - j\omega L\vec{i} \tag{21}$$

On the other hand, at the capacitor bank, the converter and grid currents are related by

$$\vec{i} - \vec{i_g} = C\frac{d\vec{v}}{dt} + j\omega C\vec{v} \tag{22}$$

This relations are used by the VCR of Fig. 2 to control the converter current. As seen in Fig. 2, the VCR calculates the reference for the PWM system ${v_c}^*$ as

$${v_{dc}}^* = k_{pc}(i_d^* - i_d) + k_{ic}x_{dc} - li_q \tag{23}$$

$${v_{qc}}^* = k_{pc}(i_q^* - i_q) + k_{ic}x_{qc} + li_d, \tag{24}$$

where k_{pc} and k_{ic} are the current controller proportional and integral gains, respectively, and the compensating cross terms have been added. x_{dc} and x_{qc} are the d-q current error states, given by

$$\frac{1}{\omega_0}\frac{dx_{dc}}{dt} = i_d^* - i_d \tag{25}$$

$$\frac{1}{\omega_0}\frac{dx_{qc}}{dt} = i_q^* - i_q \tag{26}$$

Similarly, the voltage controller input is the voltage error, while the output is the current reference, given by

$$i_q^* = k_{pv}(u_{qg}^* - u_{qg}) + k_{iv}x_{qv} - cu_{dg}, \tag{27}$$

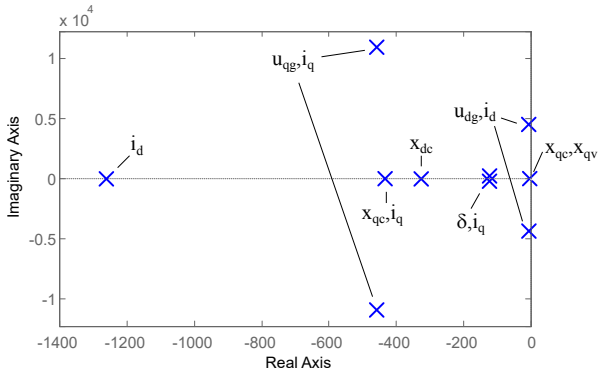

Fig. 8. Base case eigenvalues and related states according to their participation factors.

where k_{pv} and k_{pv} are the voltage controller proportional and integral gains, respectively, and the compensating cross terms have been added. As in the current controller, x_{qv} is the q voltage error state, given by:

$$\frac{1}{\omega_0}\frac{dx_{qv}}{dt} = u_{qg}^* - u_{qg} \tag{28}$$

The equations of the filter inductance, (21), and capacitance, (22), the VCR states, (25),(26) and (28), together with the power angle definition, (1), and the equation from the grid impedance, (4), form a dynamic non-linear system that can be represented in the state-space as

$$\frac{d\Delta x}{dt} = A\Delta x + B\Delta u, \tag{29}$$

, where

$$x = [u_{dg}, u_{qg}, x_{qv}, i_d, i_q, x_{dc}, x_{qc}, i_{dg}, i_{qg}, \delta] \tag{30}$$

$$u = [{i_d}^*, q^*, w_g] \tag{31}$$

B. Stability analysis

In this section, the influence of the system parameters on the loci of dominant eigenvalues is studied considering the base-case scenario given in Table III.

For this base case, the eigenvalues are computed and presented in Table IV. Frequency and damping ratio are also given, as well as the dominant states according to their participation factors. A graphical representation is presented in Fig. 8.

It can be seen that the dominant eigenvalues are related to phase and voltage amplitude variations. This validates the assumption made in section III of considering that the VCR dynamics are significantly faster than the synchronizing system ones. All the eigenvalues have a negative real part and thus the system is stable.

A common concern in synchronization systems is their sensitivity to the grid "strenght" or Short Circuit Ratio (SCR). Fig. 9.(a) shows the effect on the system eigenvalues of a grid impedance variation from 0.1 pu (low SCR) to 0.02 pu (high SCR). It can be seen how the eigenvalues related to the phase displacement δ become more damped while the frequency of the eigenvalues related to the voltage amplitude

TABLE IV
BASE-CASE EIGENVALUE ANALYSIS

λ_i	Eigenvalues [rad/s]	Frequency [Hz]	Damping ratio [pu]	Dominant states
$1-2$	$-490.6 \pm 10\,870.8$i	1730.1	0.045	u_{qg}, i_q
$3-4$	-6.1 ± 4433.0i	705.5	0.001	u_{dg}, i_{dg}
5	-1348.8	0	1	i_d
6	-459.1	0	1	x_{qv}, i_q, i_{qg}
$7-8$	-70.3 ± 208.4i	33.16	0.32	δ, i_{qg}
9	-10.5	0	1	x_{qv}, x_{qc}
10	-233.7	0	1	x_{dc}

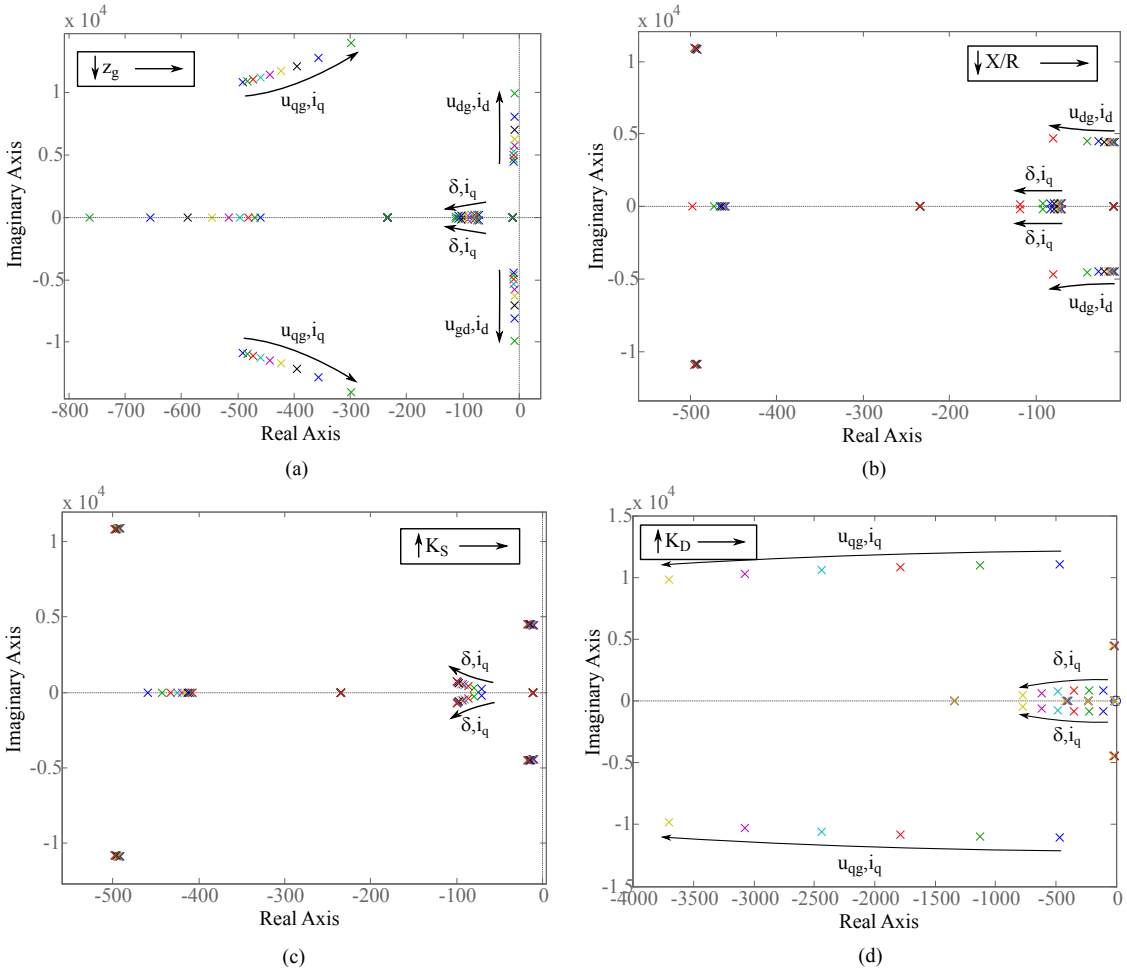

Fig. 9. System response against variations on (a) the grid impedance z_e, (b) the grid inductive to resistive ratio X/R_e, (c) the synchronization loop gain K_s and (d) the damping gain K_D.

increases. However, the system remains stable regardless of such a high variation of the grid impedance.

Another concern, specially in droop control systems, is the dependency with the grid impedance inductive or resistive behavior. This can be defined by the inductive to resistive ratio (X on R, or X/R). In most electrical systems this ratio is very high and thus grid impedance can be considered purely inductive. However, this might not be the case in microgrids, where more resistive networks are likely to appear [12].

A variation of X/R from 20 to 1 has been tested. Results are depicted in Fig. 9.(b). It can be seen how the system improves its stability for a more resistive impedance. This is due to the stronger coupling between frequency and reactive power that appears on resistive networks [13]. The resistive nature also helps to damp oscillations related to δ. However, as seen from the base case, the systems is also stable for highly inductive networks.

Besides, in order to illustrate the effect of the regulation parameter K_s, a variation from 0.1 to 1 is performed. As with other proportional control systems, this parameter must be chosen regarding both the steady-state relation between reactive power and frequency and the desired dynamic performance. From the results in Fig. 9.(c), it can be seen how the poles related to δ become faster and less damped, as expected form the characteristic swing equation (16). Thus, a compromise must be achieved between the control bandwidth and stability

margin.

C. Damping of oscillations

There are two prominent oscillations, one appearing close to Ω_b, as expected from (14), and another at around the filter resonance frequency. Since the grid resistance has been considered to be very low, this resonances are poorly damped.

The resonance related to the filter is common in VSC based systems. Its frequency is usually designed as a compromise between economic and technical parameters. Damping of these high-frequency oscillations through the control system, or active damping, is a developing topic in the literature. A comparison between some of the most common methods was recently presented in [27]. For this work, these oscillations have been passively damped with a resistor connected in series with the filter capacitor.

The low-frequency resonance appears as a direct consequence of the link established between reactive power and phase displacement, as can be deduced from (14). A similar resonance appears in [18], where the PSC was proposed, for the relation between active power and phase displacement.

In order to damp these oscillations, the authors of [18] introduce variations in the generated voltage amplitude related to the current oscillations by means of a high-pass filter. This structure for damping oscillations is similar to the traditional "washout" filter used in the excitation system of synchronous generators [28].

Here, these oscillations are compensated by introducing an opposite-sign variation in the internal phase, which is related to v_q. Since these variations will appear in i_q, measurements of i_q are used to implement the damping through v_q reference variations. A high-pass filter (HPF) is used to avoid steady-state variations. This structure is depicted in Fig. 2. The gain introduced by this HPF is

$$G_{HPF} = K_D \frac{T_w s}{1 + T_w s} \tag{32}$$

An illustrating approach to show the effect of this system, following the simplified model of section II, is studying the modification of the swing equation (16), which becomes

$$\frac{1}{K_s {\Omega_b}^2} s^2 \Delta\delta + \frac{r_g + G_{HPF}}{\omega_0 l_g K_s \Omega_b} s\Delta\delta + G_{p\delta}\Delta\delta = \Delta p^* \tag{33}$$

It can be seen how the equivalent D parameter is modified by the damping mechanism.

The effect of this system on the complete model, varying K_D from 0 to 0.5 pu, is shown in Fig. 9.(d). It can be seen how the damping of the eigenvalues related to the synchronizing system increases.

IV. Results and Discussions

In this section, the simulation and experimental results are presented to demonstrate the performance of the proposed control system as well as to validate the developed dynamic models.

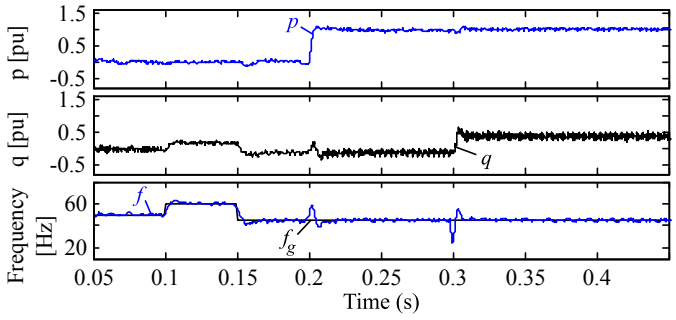

Fig. 10. Simulation results against frequency, active power reference and reactive power reference variations.

A. Simulations

Simulations were developed using a detailed switching model implemented in MATLAB/Simulink in co-simulation with PSIM. Simulink was used to implement the control system whereas PSIM was used for simulating the power system components.

The simulated system response is tested against frequency and active and reactive power reference step variations. First, the synchronizing system is tested by performing a frequency step. Then, it is demonstrated how active and reactive power can be independently controlled. To conclude, the system inherent capability to limit the VSC current under fault conditions is tested. Results are depicted in Fig. 10 and Fig. 11.

At t=0.1s. the grid frequency f_g suffers a step from 50Hz to 60Hz. It can be seen how the internal frequency of the control f, which is the representation in Hz of the angular frequency ω calculated through the RPS loop of Fig. 5, follows this change. This demonstrates that the proposed control system can track this new frequency even for such a high and sharp variation. To track this new frequency, the control system varies the reactive power reference proportionally by a K_s factor. The active power reference remains unchanged, showing that it was not needed for the synchronization process. At t=0.15s the grid frequency suffers a falling step from 60Hz to 45Hz to show that the previous variation is not a particular simulation case.

An active power reference step, from 0 to 1 pu, is performed at t=0.2s. Active power rises accordingly, showing that the control system is able to track this reference. The frequency changes during the transient, as expected from the block diagram of Fig. 6 where active power is a disturbance in the control loop. The control system is able to compensate this perturbation so the frequency f is restored to f_g and the system remains in synchronism with the grid. Note that this transient frequency variation is needed for achieving the new power angle required by the power variation

Finally, a reactive power reference step, from 0 to 0.5 pu, is performed at t=0.3s. As with active power, the control system is able to track this reference while maintaining synchronism with the grid. The final reactive power is not exactly 0.5 pu because of the open-loop configuration of the reactive power channel.

The proposed synchronization system presents the advan-

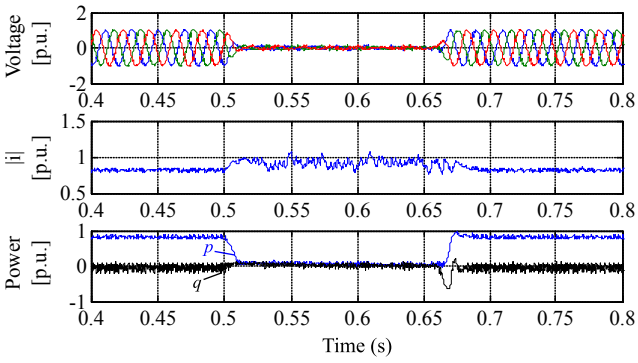

Fig. 11. Simulated system response against a grid fault.

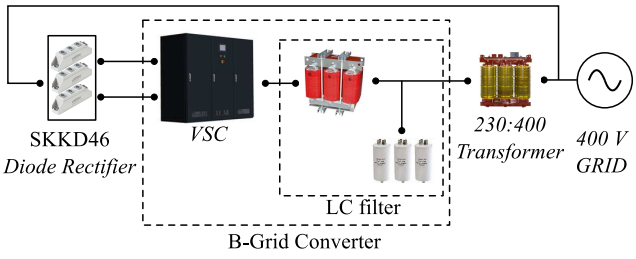

Fig. 12. Set-up configuration used in the real-time experiments.

tage of being built upon the well-known current vector control. This provides the capability of limiting the VSC current under faults without any additional systems. This capability has been tested in the proposed system as shown in Fig. 11. A fault is produced at $t = 0.5s$. The converter active current is limited, so the active power is reduced. When the fault is cleared at $t = 0.7s$, the control is able to return to pre-fault levels.

B. Experimental results

In this section, the simulation results are compared with a real-time implementation.

The diagram of experimental set-up used to obtain the real-time results is depicted in Fig. 12. An overview picture of the set-up is presented in Fig. 13. This set-up consists of a commercial three-phase two-level VSC with a rated power of 300kW and a switching frequency of 3.35kHz equal to the sampling frequency, which includes a 0.2mH/200μF LC filter.

The inverter is fed by a three-phase diode rectifier composed of three SEMIKRON SKKD46 mono-phase diode branches, in order to provide a dc bus voltage of around 550 V, which gives enough headroom to connect the inverter to a 400-V grid through a 230/400-V DY isolation transformer.

Results are shown Fig. 14. It was not possible to replicate the frequency variation presented in the simulation since the system was connected to a stiff grid. Therefore, only the response to active and reactive power variations is included. The grid frequency f_g could not be directly measured so a constant value of 50 Hz is presented as a reference.

An active power reference step is applied at t=0.2s as shown in Fig. 14.(a). As in the simulation case, the control system is able to track this reference while maintaining a constant frequency. The transient frequency variation is significantly

Fig. 13. Overview of the set-up used in the real-time experiments.

smaller than in the simulated case, probably due to the damping provided by the electrical power losses.

The response to the reactive power reference change is shown in Fig. 14.(b). It can be seen that the behavior is similar to the one expected from the simulation. The transient frequency variation is again smaller than in the simulated case. However, note that it is significantly higher than in the active power variation scenario of Fig. 14.(a), which is in accordance with the dynamic coupling studied in section II-A.

Regarding the synchronizing capabilities, it can be seen that the system behavior is similar to the one observed in simulation, validating the presented models.

V. Conclusions

This paper presents a novel synchronization strategy based on the measurement of reactive power variations. In this way, active power can be independently controlled, as opposed to droop or VSM control systems where active power is linked to the synchronizing mechanism. As in VSM systems, no measurement of the grid frequency and angle is required, in opposition to systems based on PLLs, which have indubitable advantages.

Since the proposed system is based on the well-known VOC, it presents some of its most important features, including independent active and reactive power control and current limitation capability.

In contrast to previous references that included a coupling between reactive power and frequency, in this paper the aim

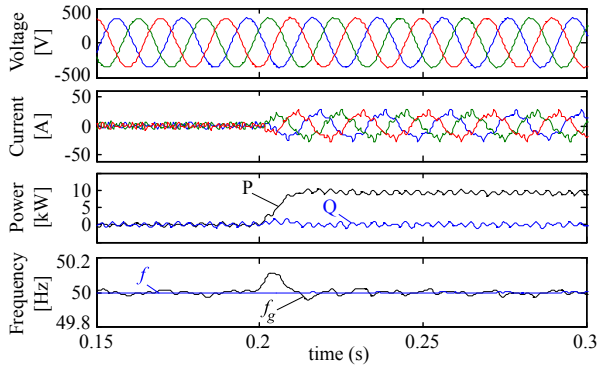

(a)

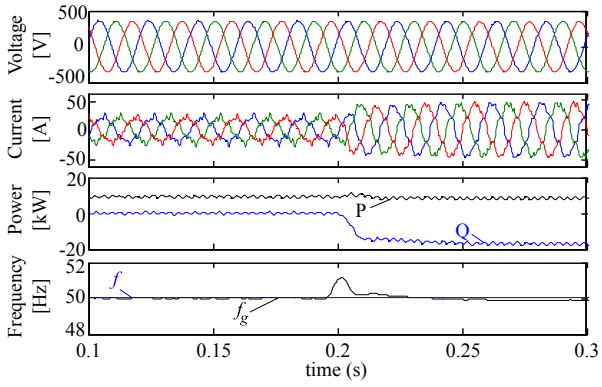

(b)

Fig. 14. Experimental results for (a) an active power reference step variation and (b) a reactive power reference step variation.

is not to share reactive power between VSCs but to synchronize a VSC to the grid. With the proposed system, active power is not required for synchronization, while in traditional power/frequency droop the synchronism is not possible if the active power required by the synchronizing mechanism is not controllable since the power/frequency droop will require active power sharing that cannot be guaranteed.

The proposed system has been modeled in the state-space. An eigenvalue analysis is presented to show the system performance in scenarios with different short circuit impedances different X/R ratios as well as strong and weak grids. Simulation and experimental results for a practical case study are presented to further validate the proposed control system.

REFERENCES

[1] R. H. Lasseter, "MicroGrids," in *IEEE Power Engineering Society Winter Meeting, 2002*, vol. 1, 2002, pp. 305–308.

[2] H. Bevrani and T. Ise, *Microgrid Dynamics and Control*. John Wiley & Sons, 2017.

[3] A. Yazdani and R. Iravani, *Voltage-Sourced Converters in Power Systems: Modeling, Control, and Applications*. Hoboken, NJ, USA: John Wiley & Sons, 2010.

[4] J. Svensson, "Synchronisation methods for grid-connected voltage source converters," *IEE Proceedings-Generation, Transmission and Distribution*, vol. 148, no. 3, pp. 229–235, 2001.

[5] F. Blaabjerg, R. Teodorescu, M. Liserre, and A. V. Timbus, "Overview of control and grid synchronization for distributed power generation systems," *IEEE Transactions on industrial electronics*, vol. 53, no. 5, pp. 1398–1409, 2006.

[6] H. Konishi, C. Takahashi, H. Kishibe, and H. Sato, "A consideration of stable operating power limits in VSC-HVDC systems," in *Seventh International Conference on AC and DC Transmission*, 2001.

[7] I. Richard, Z. Jiebei, R. Andrew J, Y. Mengran, and D. Adam, "Effects of VSM Convertor Control on Penetration Limits of Non-Synchronous Generation in the GB Power System," *15th Wind Integration Workshop, Vienna 15-17 Nov*, no. CP679, pp. 1–8, 2016.

[8] National Grid, "Performance of Phase-Locked Loop Based Converters," National Grid, Tech. Rep., 2017.

[9] M. C. Chandorkar, D. M. Divan, and R. Adapa, "Control of parallel connected inverters in standalone ac supply systems," *IEEE Transactions on Industry Applications*, vol. 29, no. 1, pp. 136–143, 1993.

[10] M. N. Marwali and A. Keyhani, "Control of distributed generation systems-Part I: Voltages and currents control," *IEEE Transactions on power electronics*, vol. 19, no. 6, pp. 1541–1550, 2004.

[11] K. De Brabandere, B. Bolsens, J. Van den Keybus, A. Woyte, J. Driesen, and R. Belmans, "A voltage and frequency droop control method for parallel inverters," *IEEE Transactions on power electronics*, vol. 22, no. 4, pp. 1107–1115, 2007.

[12] J. M. Guerrero, M. Chandorkar, T. L. Lee, and P. C. Loh, "Advanced Control Architectures for Intelligent Microgrids-Part I: Decentralized and Hierarchical Control," *IEEE Transactions on Industrial Electronics*, vol. 60, no. 4, pp. 1254–1262, Apr. 2013.

[13] Q.-C. Zhong, "Robust droop controller for accurate proportional load sharing among inverters operated in parallel," *IEEE Transactions on Industrial Electronics*, vol. 60, no. 4, pp. 1281–1290, 2013.

[14] J. W. Simpson-Porco, F. Dörfler, and F. Bullo, "Synchronization and power sharing for droop-controlled inverters in islanded microgrids," *Automatica*, vol. 49, no. 9, pp. 2603–2611, 2013.

[15] F. P. Demello, "Concepts of synchronous machine stability as affected by excitation control," in *IEEE Transactions on Power Appparatus and Systems*. Citeseer, 1969.

[16] H.-P. Beck and R. Hesse, "Virtual synchronous machine," in *Electrical Power Quality and Utilisation, 2007. EPQU 2007. 9th International Conference On*. IEEE, 2007, pp. 1–6.

[17] Q.-C. Zhong, P.-L. Nguyen, Z. Ma, and W. Sheng, "Self-synchronized synchronverters: Inverters without a dedicated synchronization unit," *IEEE Transactions on Power Electronics*, vol. 29, no. 2, pp. 617–630, 2014.

[18] L. Zhang, L. Harnefors, and H.-P. Nee, "Power-synchronization control of grid-connected voltage-source converters," *IEEE Transactions on Power systems*, vol. 25, no. 2, pp. 809–820, 2010.

[19] J. Liu, Y. Miura, and T. Ise, "Comparison of Dynamic Characteristics Between Virtual Synchronous Generator and Droop Control in Inverter-Based Distributed Generators," *IEEE Transactions on Power Electronics*, vol. 31, no. 5, pp. 3600–3611, May 2016.

[20] S. D'Arco and J. A. Suul, "Equivalence of virtual synchronous machines and frequency-droops for converter-based microgrids," *IEEE Transactions on Smart Grid*, vol. 5, no. 1, pp. 394–395, 2014.

[21] C. K. Sao and P. W. Lehn, "Control and power management of converter fed microgrids," *IEEE Transactions on Power Systems*, vol. 23, no. 3, pp. 1088–1098, 2008.

[22] J. M. Guerrero, N. Berbel, J. Matas, J. L. Sosa, J. Cruz, and A. Alentorn, "Decentralized Control for Parallel Operation of Distributed Generation," *IEEE Transactions on Industrial Electronics*, vol. 54, no. 2, pp. 1–10, 2007.

[23] H. Hanaoka, M. Nagai, and M. Yanagisawa, "Development of a novel parallel redundant UPS," *Telecommunications Energy Conference, 2003. INTELEC'03. The 25th International*, pp. 493–498, 2003.

[24] E. A. A. Coelho, P. C. Cortizo, and P. F. D. Garcia, "Small-signal stability for parallel-connected inverters in stand-alone AC supply systems," *IEEE Transactions on Industry Applications*, vol. 38, no. 2, pp. 533–542, Mar. 2002.

[25] N. Pogaku, M. Prodanovic, and T. C. Green, "Modeling, Analysis and Testing of Autonomous Operation of an Inverter-Based Microgrid," *IEEE Transactions on Power Electronics*, vol. 22, no. 2, pp. 613–625, Mar. 2007.

[26] A. P. n. Asensio, S. A. Gómez, J. L. Rodriguez-Amenedo, M. G. Plaza, J. E.-G. Carrasco, and J. M. A.-M. de las Morenas, "A Voltage and Frequency Control Strategy for Stand-Alone Full Converter Wind Energy Conversion Systems," *Energies*, vol. 11, no. 3, pp. 1–19, 2018.

[27] J. Roldán-Pérez, E. J. Bueno, R. Peña-Alzola, and A. Rodríguez-Cabero, "All-Pass-Filter-based Active Damping for VSCs with LCL Filters Connected to Weak Grids," *IEEE Transactions on Power Electronics*, vol. PP, no. 99, pp. 1–1, 2018.

[28] P. Kundur, N. J. Balu, and M. G. Lauby, *Power System Stability and Control*. McGraw-hill New York, 1994, vol. 7.